NEXT GENERATION ROBUST LOW-NOISE SEISMOMETER FOR NUCLEAR MONITORING

Igor A. Abramovich and Tao Zhu

PMD Scientific, Inc.

Sponsored by the National Nuclear Security Administration

Award No. DE-FG02-07ER84738

ABSTRACT

Effective global monitoring of nuclear explosions calls for a worldwide network of seismic stations equipped with the next generation high quality digital seismometers for nuclear monitoring recording data in the 0.02–16Hz band. This project addresses these requirements: it is aimed at the implementation of the next generation, very low noise, broadband, wide dynamic range, robust force-balanced digital seismometer for seismic monitoring of nuclear explosions. Successful completion of Phases II of this project will serve vital national interests in greatly facilitating global compliance with nuclear non-proliferation and detection of possible violations of the Comprehensive Nuclear-Test-Ban Treaty by rogue states.

The new seismometers should also be competitive in various niches of the worldwide seismic market due to their valuable combination of high performance, especially the low noise over broad passband, and ruggedness.
The new generation seismometer will use improved electrochemical transducers built into three similar orthogonally mounted sensors, the latter based on conceptually new design ideas that, when implemented, will result in a drastic increase in signal to noise ratio. The principles of operation and detailed noise analysis of electrochemical motion sensors are presented along with the explanation of how such major noise reduction can be achieved. The new concept has already shown to be promising based on test results of the experimental sensor prototypes.
The new instruments will be deployable in field and stationary vault environments; they will be highly reliable and offer low cost of ownership since they require no maintenance: no mass locks; no mass position monitoring and/or mass centering over the full temperature range of -12 to +60C. No break-out boxes are needed. The rugged design will greatly reduce probability of damaging such instruments during transportation and handling. The seismometer will incorporate a high-resolution, low noise, very low power versatile 24-bit digitizer that will provide digital outputs with velocity-flat and optional acceleration flat and combined velocity/acceleration-flat response. The noise level of the proposed seismometers should be at least 10dB below the USGS New Low Earth Noise Model with the dynamic range of no less than 136dB over the 0.02 to 16Hz frequency band. Maintaining the wide dynamic range, the uniform frequency response over the passband, and the considerably reduced noise will be facilitated by the use of the efficient force-balancing electrodynamic feedback. At major developmental milestones the prototype instruments will be vault-tested side-by-side with STS2 seismometers. The complete digital seismometer is expected to consume less than 750mW.

OBJECTIVES

An advanced digital seismometer with the following features that are in full compliance with the goals set forth in the Phase I proposal and also, where possible, with the CTBTO “Minimum Requirements” (CTBT/PC/II/I/Add. 2) and AFTAC additional recommendations will be built:

- **Ruggedness**: the instrument will be able to survive and remain fully operational after a shock of ≥50g for 10ms. No mass locking mechanism will be used.
- **No Maintenance Operation:** no mass position monitoring and no mass centering will be required over the full operating temperature range.
- **Passband:** 0.02 – 16Hz.
  The passband will be defined by the -3 dB corner frequencies with the ripple in gain of no more than +/- 1 dB from the mean gain values as measured from one octave above the lower corner frequency to one octave below the upper corner frequency
- **Sensor Response:** Two sets of analog and/or digital outputs will be provided concurrently: velocity-flat and acceleration-flat over the passband. A ‘hybrid’ response utilizing the combination of both will also be available.
- **Seismometer Noise:** These objectives were set forth in Phase I Proposal:

Passband	Target Noise Level
0.02-0.1Hz	-185 -190dB – *below NLNM*
0.1 – 6Hz	-185 -190dB – *below NLNM*
6 – 16Hz	(-185 -190) –180dB – *below NLNM*

- **Calibration:** Within 5% in amplitude and 5º in phase over the passband referenced to the theoretical transfer function model.
- **Limited Leveling:** the sensor will stay fully operational at installation tilts of at least ±8°.
- **Application Types:** Field, vault, borehole.
- **Environmental:**
  - **Operating Temperature Range:** -12 to +65C.
  - **Fully Hermetical, Pressurized:** the land-based seismometer will remain fully operational when submerged to the depth of at least 2m or up to 20m when equipped with an underwater type connector. The borehole version will be designed to be fully operational in the flooded boreholes down to 100m (>10kg/cm^2)
- **Robust borehole seismometer**: A robust ≤6” diameter borehole seismometer with all of the above characteristics.

The following specifications relate to the digitizer that will be integrated into the proposed seismometer. This digitizer will be a significantly upgraded version of the present PMD Scientific Series SD6503.

- **Digitizer Sampling Rate**: programmable up to at least 100sps while complying with the noise specifications below.
- **Digitizer Resolution:** 12dB below the seismometer noise.
- **Digitizer Noise Referenced to its Input:** 10dB below the seismometer noise.
- **System Dynamic Range:** ≥ 135dB
- **Absolute Timing Accuracy**: better than ±0.5ms relative to the external GPS receiver
- **System Total Power Consumption:** <0.7W
- **Optional**: digital data storage, SATA SSD flash disk up to 32GB
- **Optional**: LAN connection

A. Sensor description

A typical electrochemical sensor (Figure 1) has a plastic housing filled with strong electrolytic solution: potassium iodide, *KI*, with a small addition of iodine, I_2. Electrolyte is contained between a pair of elastic membranes that significantly contribute to the sensor’s transfer function. The transducer consists of four fine platinum mesh electrodes, two anodes, and two cathodes, separated by thin polymer mesh or laser-perforated mica spacers. The stack is tightly held together between two flanges. The motion of the fluid caused by an external acceleration is converted into an electrical signal via convective diffusion of the ions in the electrolyte. When a small dc offset is applied between the anodes and cathodes, the flow of ions of each type can be described by the following expression (Newman, 1973; Koryta, 1993):

$$\mathbf{j}_a = -D \cdot \nabla c_a + q_a \cdot c_a \cdot \mu \cdot \mathbf{E} \tag{1}$$

Where D = diffusion coefficient; μ = mobility and c_a = concentration of active ions; **E** = the electrical field vector. Since the strong electrolyte is an excellent conductor, the electric potential drops rapidly in the vicinity of the electrodes, and there is no electric field in the bulk of the fluid. Thus the second term in Equation 1 can therefore be ignored. Therefore, the application of a bias voltage results *only* in a concentration gradient. An acceleration, **a,** along the channel creates a pressure differential, **ΔP,** across the transducer, which forces the liquid to move with a velocity, **v**. This flow of electrolyte entrains ions and causes an additional charge transfer between the electrodes:

$$\mathbf{j}'_{\mathbf{a}} = \mathbf{v} \cdot c_a \tag{2}$$

The total current from active ions, in the presence of acceleration, can be expressed as:

$$\mathbf{j}_{\mathbf{a}} = -D \cdot \nabla c_a + \mathbf{v} \cdot c_a \tag{3}$$

Thus the transducer generates an electrical signal in response to acceleration.

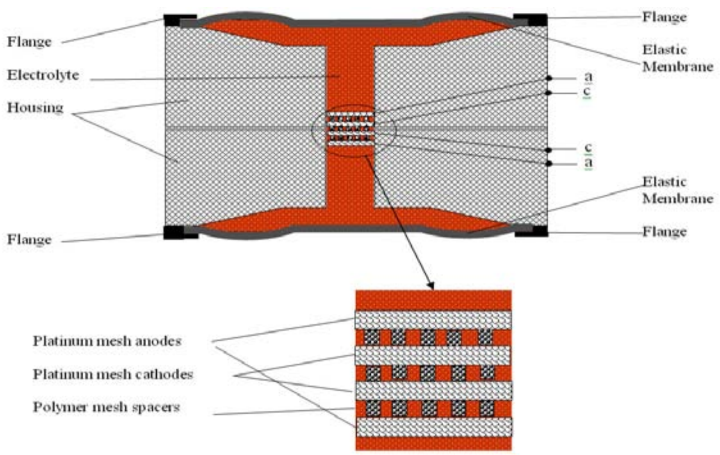

Figure 1. A Basic Electrochemical Seismic Sensor.

A general expression describing noise in units of external acceleration (derived in by PMD consultant Dr. K. Sakharov [1992]):

$$\left\langle a^2 \right\rangle_\omega = \frac{2R_h kT}{(\rho L)^2} \tag{4}$$

Where: ρ = electrolyte density; L = electrolyte effective length in the direction of the acceleration; k = Boltzmann constant; T = absolute temperature; R_h = hydraulic impedance. The nominator in Equation 4 represents hydrodynamic thermal noise, similar to the Nyquist noise in electric circuits with the R_h standing for the electric resistance R (Van der Ziel, 1970). The total noise of a sensor agrees with Equation 4 only in the mid-frequency region. The elevated noise spectral density at both ends of the passband is due to at least two addition sources. The additional noise is unavoidable even when the two halves of the transducer are exactly symmetrical and thus their noise components add up to zero at the transducer differential output. These two sources are: fluctuation noise of the current flowing in the transducer; noise of the electronic amplifiers

The spectral density of fluctuation noise is described by the general equation:

$$\left\langle I^2 \right\rangle_\omega = 2qI \tag{5}$$

Where I = quiescent current of the transducer cell(Abramovich, 1992–94):

$$I = \frac{Dc_0 eS}{l}\left(1 - \exp(-\frac{qU_0}{kT})\right) \tag{6}$$

q = elementary charge in the cell. As two electrons participate in each elementary charge exchange reaction at the electrodes, $q = 2e$; D = diffusion coefficient; c_0 = charge carriers equilibrium volumetric concentration; U_0—voltage between and S = effective area of the electrodes; l = distance between the electrodes. Since each transducer consists of two independently working identical cells that are together characterized by the transfer function W, the following equation describes sensor fluctuation noise in units of acceleration:

$$\left\langle a^2 \right\rangle_\omega = {8eI}\Big/{\left(W/\omega\right)^2} \qquad (7)$$

The practical method of increasing the signal-to-noise ratio is an addition of an inertial mass. For example, vertical and horizontal sensors of the PMD BB603 broadband seismometer are equipped with ~650g masses which results in noise below NLNM in the 0.06–8Hz. To account for the additional mass Equation 4 is modified:

$$\left\langle a^2 \right\rangle_\omega = \frac{2R_h kT}{\left(\rho L + M/S_s\right)^2} \qquad (8)$$

Where M = external mass and S_s = effective area of the sensor membrane. This is a simple, proven approach; it is easy to change/adjust M; the additional mass ("frame") is mounted in such a way that the membranes are not deformed. The frame carries a voice coil that transmits the feedback force to the membrane. Both qualitative and quantitative validity of Equation 8 have been confirmed experimentally. Evidently, further increase of the inertial mass would be impractical.

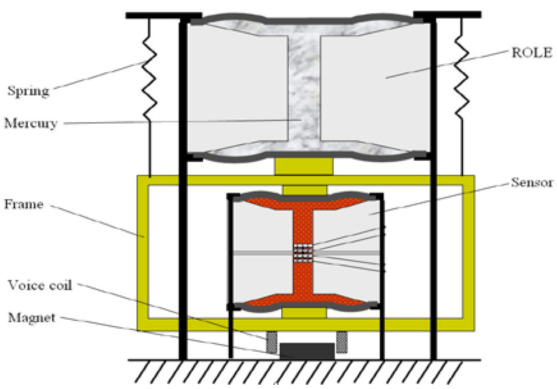

Figure 2: HEX design concept

To achieve the required noise levels a radically new approach was necessary. While there is no known electrolyte with much higher density, a well known exceptionally heavy liquid exists: ***mercury*** (13.6 g/cm^3). The conceptual design of a sensor that we called HEX ('**H**ybrid **E**lectro-**C**hemical **S**ensor') is shown in Figure 2. A smaller electrochemical sensor has a flame with a voice coil moving around a magnet working in the force-balancing loop. The frame's top is firmly tied to the lower membrane of a larger sensor-like structure filled with mercury. The frame in such structure performs several functions: it carries the voice coil and thus transfers the balancing force to the sensor; it transfers pressure from the upper to the lower device; finally, it is attached to the suspension springs that balance the weight of the total oscillatory mass consisting of the frame itself, mercury and electrolyte. An external acceleration along the sensitive axis is transformed into pressure differential, ΔP_i, between membranes in each of the two pairs: the large upper and the small lower. The following equation describes HEX noise:

$$\left\langle a^2 \right\rangle_\omega = \frac{2R_h kT}{\left(\rho_m h_m \dfrac{S_m}{S_s}\right)^2} \qquad (9)$$

Where ρ_m and h_m are respectively density and column height of mercury and S_m = area of the ROLE membrane (we called the mercury-filled device 'ROLE' – short for '**ρ**-**L**-**E**nhancer': see ρ, L terms in Equation 1). For a more detailed description of this sensor's principle of operation along with the derivation of the above equation see work plan section below.

Comparison of Equations 4 and 9 shows that the new concept not only capitalizes on the very high density of mercury, but achieves more than that: since the <u>noise is inversely proportional to the ratio of the diameters of the two membranes it is possible to achieve an even larger increase in signal-to-noise ratio</u>.

B. HEX Sensor Operating Principle

An external acceleration component acting along the device sensitive axis is transformed into pressure differential, $\boldsymbol{\Delta P_i}$, between membranes in each of the two pairs: the large (upper) and the small (lower) ones. For each pair, $\Delta P_i = \rho_i \cdot \ddot{x} \cdot h_i$ where ρ_i = liquid's density; $\ddot{x}$ = acceleration; and h_i = height. Force with which the lower membrane of the top structure acts on the frame, $F = \Delta P_m \cdot S_m$. The frame applies this force to the smaller sensor membrane and thus generates an additional pressure differential $\boldsymbol{\Delta P_{add}}$:

$$\Delta P_{add} = \frac{F + m_f \cdot \ddot{x}}{S_s} = \left(\rho_m \cdot h_m \frac{S_m}{S_s} + m_f \right) \cdot \ddot{x} \qquad (10)$$

Where $m_{f=}$ mass of the frame; S_m and S_s = areas of the larger and smaller membranes respectively; ***Hg*** specific gravity $\rho_m = 13600 kg/m^3$; h_m= height of the column of ***Hg***. It is important to notice that the *mass* of mercury does not enter into Equation 20, only the *height of its column*. Signal developed in the electrochemical transducer is proportional to the volumetric velocity, q, of the electrolyte that obeys the Darcy's Law:

$$q = -\Delta P / R_h \qquad (11)$$

As follows directly from Equation10, the signal will increase proportionally to

$$N = \frac{\Delta P_{add} + \Delta P_s}{\Delta P_s} \qquad (12)$$

The HEX noise expressed in acceleration units can now be written as:

$$\left\langle a^2 \right\rangle_{\omega} = \frac{2R_h kT}{\left(\rho_e h_e + \frac{m_f}{S_s} + \rho_m h_m \frac{S_m}{S_s} \right)^2} \approx \frac{2R_h kT}{\left(\rho_m h_m \frac{S_m}{S_s} \right)^2} \qquad (13)$$

Where ρ_e, h_e = density and column height of the electrolyte. Evidently the bigger the difference between the diameters of the larger and smaller membranes the more compact is HEX for a given noise level. The first term in the denominator is at least an order of magnitude smaller than the third and thus can be omitted. Finally, it is also evident that no practically feasible increase of the mass of the frame will contribute noticeably to the noise reduction; therefore the second term can also be deleted which results in the simplified Equation 6 above.

RESEARCH ACCOMPLISHED

A. Practical Implementation of the Noise Reduction Concept

The goal is to achieve the maximum possible noise reduction effect without sacrificing seismometer manufacturability and portability. Evidently, the following three parameters in the Equation 9 can be played with: the height of the ROLE, h_m and areas of the two membranes, S_m and S_s. The height cannot be made too large without significant increase in the overall dimensions of the instrument. Based on practical considerations, h_m should be selected equal to about 40mm. There are two factors limiting the value of S_m: the overall size and weight of the instrument and a possible pear-shaped sagging of these larger membranes in horizontal and their gravitational deformation in vertical sensors. At the same time, it is important to keep in mind that in order to achieve proper long period response the membranes cannot be made too rigid to alleviate these effects. Based on our experience, the maximum practical diameter of the larger membrane is ≤100mm. The sensor's membrane, on the other hand, should be made as small as possible. However, the smaller this membrane the more difficult it is to maintain its softness. This situation, however, changed dramatically when after many years of fruitless search we found the new membrane material, Santoprene, an elastomer alloy of EPDM rubber and polypropylene. Now it appears possible to design membranes with optimized rigidity and diameter at least as small as but most probably smaller than that of the membranes in the present smaller sensors (34mm). Indeed we hoped to construct a membrane with diameter as small as 25mm and did so in the Phase I effort. Unfortunately our first attempt to make such a membrane ended in failure: in our desire to make it much softer we went too far. The bell-shaped channel ("goffer") turned out to be too deep and the membrane was mechanically unstable. Please refer to the "Mini-Membranes" section below. If we use our standard 50mm membranes in ROLE device a 2:1 diameter ratio of the ROLE and sensor membranes becomes achievable. This choice of the geometries of both devices, as we hoped, should result in the most limited rise of the noise curve on the both ends of the passband at the same time yielding the desired noise reduction. Also, in doing so, the overall instrument dimensions should remain manageable. Based on multiple experiments, the noise of a standard transducer in a 35mm high sensor was determined to be about -155dB. Then according to Equation 9 the proposed device noise in the flat part of the passband will be:

$$\left\langle a^2 \right\rangle_{\omega} = -155 + 20\log \frac{\rho_e h_e}{\left(\rho_m h_m \dfrac{S_m}{S_s}\right)} \approx -155 + 20\log \frac{1.25 \cdot 0.035}{\left(13.6 \cdot 0.04 \cdot 2^2\right)} \approx -190dB$$

This number should be looked at with cautious optimism: on one hand, when decreasing the sensor's noise so drastically we are entering into *terra incognita*, where one should anticipate unexpected noise sources to reveal themselves, some of which are discussed in the next section. On the other hand, we can conceivably increase diameter of the ROLE membrane by a factor of, say, 1.5. This would yield an additional 6dB in noise reduction. Results of the tests performed at ASL showed exceptionally accurate estimate of noise level at long periods (due to the above mentioned instability of the 25mm Santoprene membranes, a standard sensor with 34mm membranes was used):

$$-155 + 20\log\left[1.25 \cdot 0.035 / \left(13.6 \cdot 0.04 \cdot \left(0.05/0.035\right)^2\right)\right] = \text{-183dB}$$

At the same time, noise very sharply went up starting at approximately 1Hz toward the higher frequencies, on one hand, and less steeply toward the long periods, on the other. This phenomenon has been and continues to be thoroughly investigated. Though poor suspension quite certainly played a negative role, an identical suspension was employed in the electrodynamic test sensor with noticeably better results (of course in the higher frequency range only). On the other hand, the latter should by definition generate ever stronger signal with increasing frequency, and it is possible that the lower noise was due to higher signal-to-noise ratio as compared with the HEX sensor.

B. Mini-membranes

The main conclusion drawn from both the Phase I project and the first year of the Phase II effort is that the general HEX concept is valid though several problems have been encountered. Because of this conclusion we attempted to build the next generation prototype using electrochemical sensor with significantly smaller membranes. The initial attempt though was unsuccessful due to the design flaw in smaller membranes: in trying to make the membrane as soft as possible we made central isle of the membrane way too small to allow for a stable mechanical connection between ROLE and the sensor. Therefore we asked the manufacturer (Aero Rubber Co., Tinly Park, IL) to modify the mold. Original and modified mini-membranes along with the bigger one used on all previously tested sensors are shown in Figure 3:

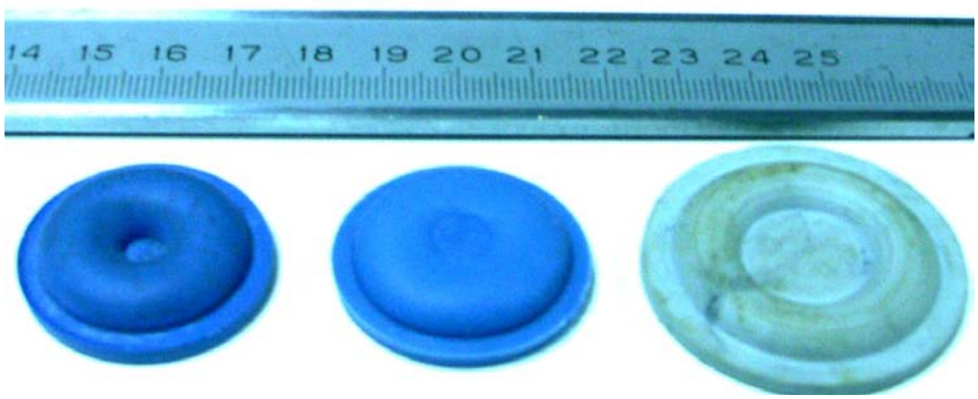

Figure 3. Left to right: original mini-membrane; modified mini-membrane; standard small membrane used in the first test sensor at the ASL.

The only difference between the two mini-membranes is that in the second one the center isle is twice as thick and therefore has a larger surface area. This modification took a very long time (over 2.5 months) but gave us a chance to do a very productive in-depth analysis of the initial prototypes design and behavior and also analyze and test a couple of modified sensor configurations. As a result, building of the next generation prototype with mini-membrane equipped sensors was delayed. Finally, we received several modified membranes (in the middle of Figure 3).

C. In-Depth Analysis of Prototype HEX Sensors

The limited time of Phase I project did not allow for a more thorough investigation of the HEX sensor properties; indeed we had concentrated totally on achieving the lowest possible noise levels without properly analyzing (and thus understanding) why, for example, we failed in getting the desired noise in the higher frequency region and, to our disappointment also at the lowest frequency when using the 25mm membranes. Designing a very complex device as HEX sensor turned out to be exceptionally time consuming and every finished prototype would be quickly calibrated and subjected to comparative noise testing. This is why in the Phase II effort we decided to first achieve a complete understanding of the device operation before undertaking any radical re-designs no matter how enticing one or another concept may seem.

Our standard quick calibration procedure yields values of R-C frequency correction components to substitute the selected standard initial values. As a rule, the second round of calibration results in the desired transfer functions. Data from intermediate calculation stages are not displayed. This time we used the unabridged procedure that allowed us to see results at every step. We were immediately puzzled by the shape of the sensor frequency response (sensor per se – without electronics) that contained two pronounced resonance peaks with a valley between them. The valley occupied just the region from a few Hertz up – right from the lowest noise valley to where HEX sensors demonstrated sharply increased noise. Thus the elevated noise was revealed but not yet understood.

Standard electrochemical sensors show bell-shaped frequency responses. We have known however that there are always two overlapping resonances: mechanical and electrochemical. The mechanical characteristic is described by a well known equation:

$$m \cdot \ddot{x} + D \cdot \dot{x} + K \cdot x = m \cdot \ddot{w} \qquad (14)$$

Where m = inertial mass; D – damping coefficient; and K=suspension rate. In our case the hydraulic impedance of the sensor provides the damping while the membranes account for about 80% of the suspension rate (the remaining 20% are provided by the spring(s)).

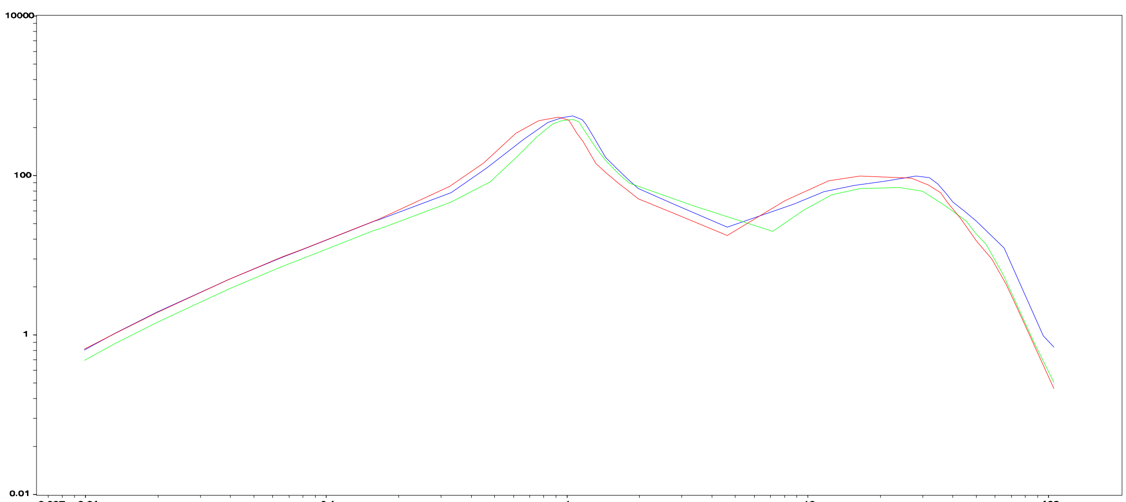

Figure 4. Sensors Frequency Responses.

The electrochemical transfer function, $W(q,\omega) = I(\omega,q)/q$, describes dependence of the transducer cell output current, I, on the external harmonic flow, q, and assumes different forms at limiting values of low and high frequency. When the system is exposed to weak low frequency flows, there is sufficient time for the formation of the diffusion layer and the current is proportional to the amount of electrolyte that flows through the electrodes. The characteristic parameter of such system is the time required for the formation of the diffusion layer: $\tau_0 \sim {(2d)^2}/{D}$, where d=½ of the distance between electrodes; D=diffusion coefficient. The transfer function, $W(q)$, will be increasing at frequencies $\omega < \omega_0 \sim 1/\tau_0$ and decreasing at $\omega > \omega_0 \sim 1/\tau_0$. At sufficiently high frequencies, when the distribution of concentration is determined by the rate of change of the signal, there is not enough time for the diffusion layer to form and because of that the output current is proportional to both the amount of electrolyte flown through the cell and the ratio of the signal change time to that of the diffusion layer formation. As a result, in this frequency region the transfer function decreases reversely proportionally to ω.

The two resonance peaks were almost indistinguishably close to each other. With the introduction of the ROLE device the relationship between the two resonances changes drastically and now we see two hills and a valley. While the feedback and electronic correction smooth and flatten this response, the valley is positioned right where it does the damage in terms of the high frequency noise.

While analyzing the HEX sensor behavior we also tested a few modifications of the original prototypes. In Figure 4 three plots are shown representing frequency responses of various modifications. The blue curve shows the response of the initial Phase 2 prototype. The green curve belongs to the HEX assembly where channel diameter in the ROLE device was increased by 35%. Finally, the red plot shows the response of the HEX similar to the previous one but with much softer ROLE membranes. Neither modification resulted in a radical improvement though the last one shows some shift of the whole response toward the lower frequencies thus promising some reduction of the noise at low and, quite unexpectedly, also at higher frequencies. Both increases though still do not lead to the target noise levels.

We also attempted to further flatten the response by employing an additional damping: a low impedance coil and a magnet (see magnetic system – 'Damping/EM Sensor' – at the bottom, below the electrochemical sensor in Figure 5; a similar but modified magnetic system was used in later experiments with additional electrodynamic sensor). Such damping did not result in any noticeable response changes. Evidently, the hydrodynamic damping effect of the sensor was at least an order of magnitude, and probably more than that, stronger than any electromagnetic damping we could implement within the design constrains of the existing prototype.

Presently practically all hydraulic impedance of the HEX system, essentially the very parameter that is responsible for the steepness of the main resonance peak, is concentrated inside the electrochemical sensor. It appears that a more beneficial result will be achieved is we decrease the sensor's impedance and increase that of the ROLE device. We can reduce diameter of the channel in the ROLE as much as it is practically possible and, in turn, double the diameter of the transducer cell thus decreasing its impedance by the factor of 16. Now at about the same noise level the membranes will not be deforming and the pressure will be transferred more uniformly from ROLE to the sensor in the passband of interest. Actually this approach is prompted at least in part by the plots in Figure 4. In combination with the use of smaller membranes in the sensor and thus overall increase in the signal-to-noise ratio this may conceivably bring us close – or directly to the target noise levels. Such modified sensor is presently being tested. The main difficulty should be anticipated in preventing the parasitic lateral electrolyte motion (lateral convection) across the electrodes. Such convection leads to a noticeable noise increase. On the other hand, we have some experience in building experimental low R_h transducers; a couple of them were tested successfully at Berkeley several years ago.

Another test prototype has been build using the smaller membranes (25mm). This time the result was more predictable since we have accumulated significant understanding of various factors impacting the HEX sensor behavior. The signal at the main resonance frequency was stronger in full compliance with the Equation 9. On the other hand, the resonance peak was much sharper. As a result, we achieved a very low noise at around the main resonance peak and even stronger noise at either end of the passband. This problem is being addressed presently and several measures are being considered; in particular changing the transducer design by using laser-perforated mica spacers instead of the polymer mesh ones. This should result in more compact transducer (due to the fact that mica is thin and exceptionally flat while the mesh has quite uneven microstructure). Then the possibility of the parasitic convection will be conceivably nil and the long period noise should go down significantly. Since these transducers are being tested right now, we cannot yet report experimental results.

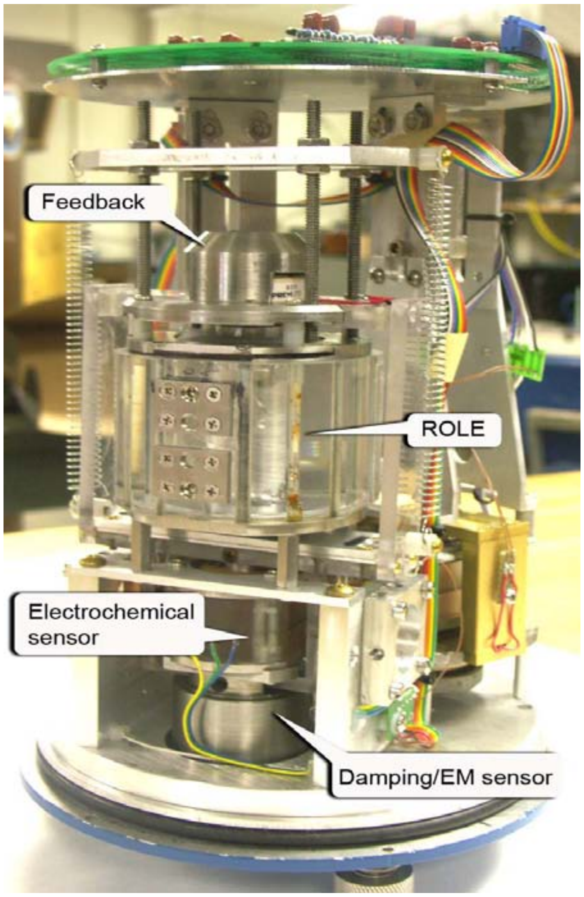

Figure 5. The latest prototype HEX sensor. A standard electrochemical sensor with large inertial mass is seen behind the HEX. Placing both sensors on a common base and in the same housing allows for very accurate correlation calculations.

Another test prototype has been build using the smaller membranes (25mm). This time the result was more predictable since we have accumulated significant understanding of various factors impacting the HEX sensor behavior. The signal at the main resonance frequency was stronger in full compliance with the Equation 9. On the other hand, the resonance peak was much sharper. As a result, we achieved a very low noise at around the main resonance peak and even stronger noise at either end of the passband. This problem is being addressed presently and several measures are being considered; in particular changing the transducer design by using laser-perforated mica spacers instead of the polymer mesh ones. This should result in more compact transducer (due to the fact that mica is thin and exceptionally flat while the mesh has quite uneven microstructure). Then the possibility of the parasitic convection will be conceivably nil and the long period noise should go down significantly. Since these transducers are being tested right now, we cannot yet report experimental results.

D. The EC/EM Combination Sensor

If the above approach turns out to be insufficient in terms of achieving the target noise levels at higher frequencies, we can turn to using the combination sensor. We tested a HEX equipped with an additional electro-dynamic transducer. The inscription in Figure 5: (“Damping/EM Sensor”) emphasizes that the magnetic system shown may contain either a damper or an electromagnetic sensor. The simpler combination we tested was an open-loop system and no special efforts were spent to achieve a flat response. However, as one can clearly see from the plots below in Figure 6, the resulting response is more manageable as compared to those shown in Figure 4 and may be readily flattened in a closed loop configuration.

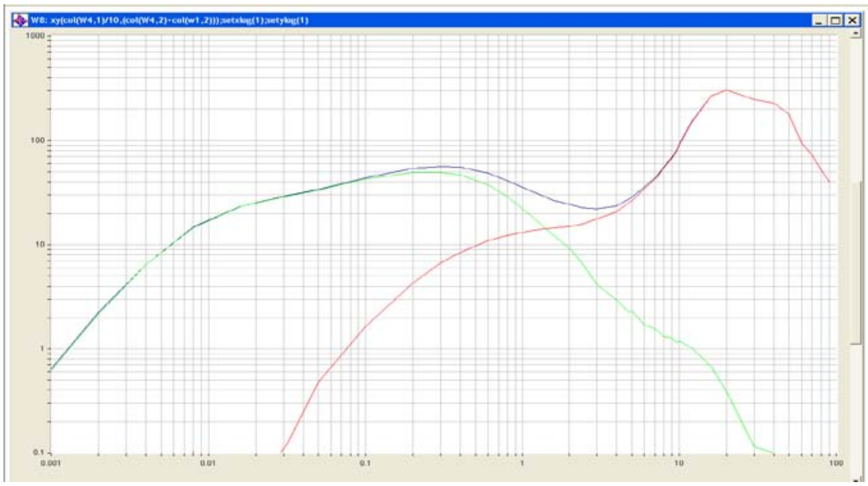

Figure 6. The Electrochemical/electrodynamic combination sensor response: green – electrochemical; red – electrodynamic; blue – combined response.

E. The Electrochemical "Gyro" sensor

This is the most exotic but quite realistic device despite its seeming complexity. We have been working on this design for a several years unrelated to any government-sponsored projects. We think it is unlikely that we will have time to incorporate this "gyro" sensor into the HEX device within the remaining year but we determined to do it rather sooner than later.

1. Concept

This unusual sensor configuration was conceived during the development of our rotational seismometer with magneto-hydrodynamic (MHD) feedback presently manufactured commercially.

In order to test the concept (see sketch in Figure 7) we modified our standard rotational sensor by adding a transverse tube. The ring contains a conventional electrochemical transducer and an MHD cell (that works as force-balancing feedback in rotational sensor). This cell consists of a pair of platinum electrodes inside the channel and a pair of strong Neodymium magnets. When a *dc* voltage is applied to the electrodes, the cell moves the strongly conductive electrolyte along the ring (solid arrow). A ground motion component along the sensitivity axis causes electrolyte to flow in/out of the main ring (dashed lines). This, in turn, effectively modulates the steady motion of the electrolyte through the transducer cell and results in a signal proportional to the ground motion velocity. Our experiments demonstrate that such sensor yields at least twice as strong signal at low and four times stronger at high frequencies than a standard electrochemical sensor. Moreover, even the open-loop system shown has close to the same linearity as our standard force-balanced instruments. The signal-to-noise ratio of this sensor can be increased even further by adding a second MHD cell and still further – the second transducer cell. Finally, due to the strong high frequency signal yield such sensor would be paired response-wise more readily and smoothly with an electro-dynamic sensor, if necessary.

Figure 8 shows the way a Gyro sensor can be built into a standard one with membranes and thus be equipped with a feedback and an inertial mass or ROLE, if desired.

While the configuration in Figure 8 may seem too complicated to make, it is actually a combination, with some additions, of our standard translational and rotational seismometers and as such it will not require any above usual design efforts be they mechanical or electronic. As for the size of the Gyro sensor, it would be actually much smaller that it may seem from observing the sketches where various dimensions were intentionally stretched in order to explain the principles of operation more clearly.

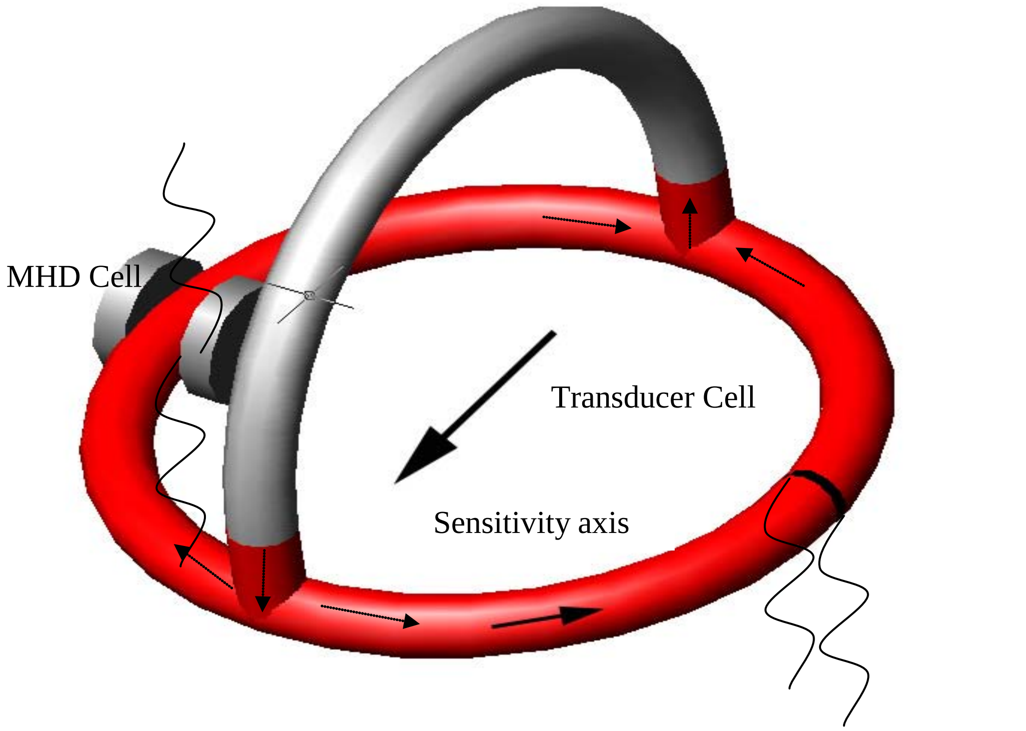

Figure 7. The Gyro type electrochemical sensor

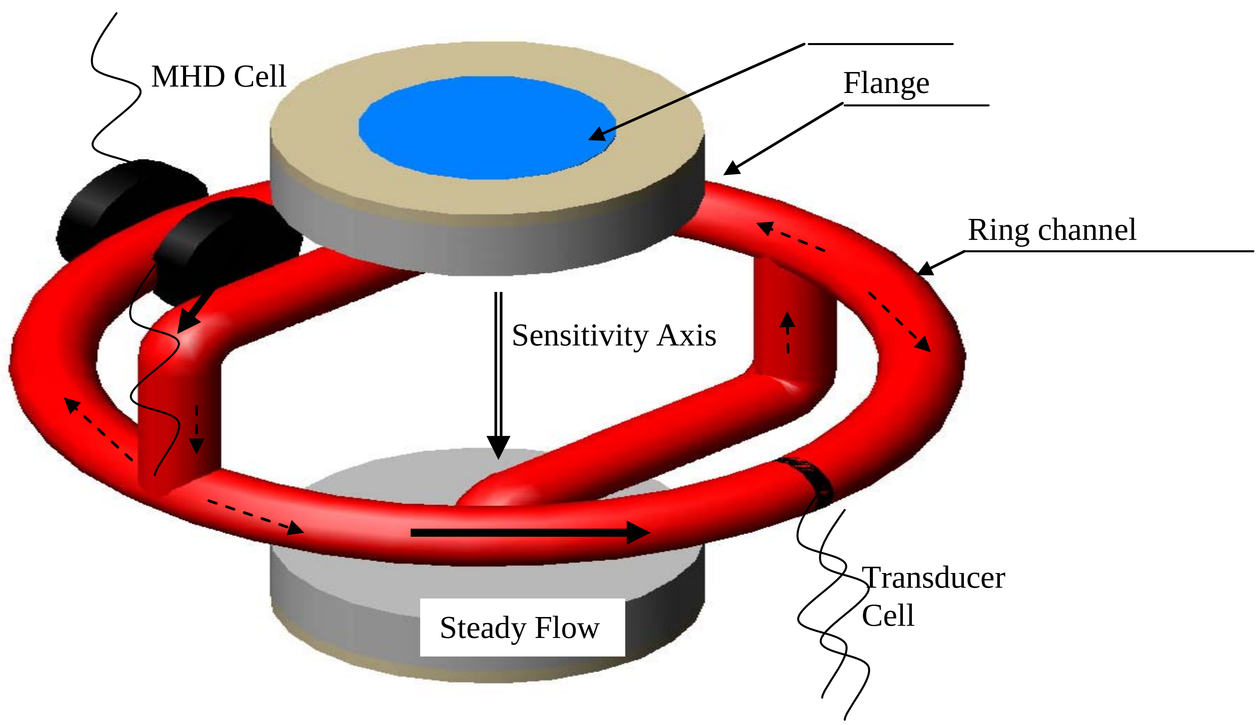

Figure 8. Sketch of a Gyro sensor ready for the addition of feedback and ROLE device.

2. *Theory of Operation*

The subject of the discussion below is an electrochemical transducer with flat mesh electrodes through with electrolyte flows with velocity

$$V = V_C + V_0 \exp(i\omega t) \qquad (15)$$

where $V_C = const.$

Operation of an electrochemical transducer is described the convective diffusion equation; for this sensor configuration it can be considered single-dimensional:

$$\frac{\partial n}{\partial t} - D\frac{\partial^2 n}{\partial x^2} = -V\frac{\partial n}{\partial x} \qquad (16)$$

With two boundary conditions:

1) Nernst relationship:

$$\frac{n_{-d}}{n_d} = \exp\left(\frac{eU}{kT}\right) \qquad (17)$$

2) Preservation of equilibrium concentration at the anode:

$$n_{-d} = n_0 \qquad (18)$$

Where n_0=concentration far away from the electrodes; U=voltage between the electrodes; n_{-d} and n_d= concentrations at the anode and cathode respectively. Solution of the equation results in the following expression[1] for the current flowing through the cathode:

$$I = -esD\frac{\partial n}{\partial x}\bigg| - esD\frac{\partial n}{\partial x}\bigg|_{x=d} = -esD\frac{\partial n_c}{\partial x}\bigg|_{x=d} - esD\frac{\partial c}{\partial x}\bigg|_{x=d} = I_C + I_W \qquad (19)$$

Where:

$$I_C = \frac{eSn_0V_C}{2sh(2R_C)}\left(\exp\left(-\frac{eU}{kT}\right) - 1\right)\exp(2R_C) \qquad (20)$$

And

$$I_W = -\frac{eSn_0V_C}{2sh(2R_C)}\left(\exp\left(-\frac{eU}{kT}\right) - 1\right)\frac{V_0\exp(i\omega t)}{i\omega d}\left((R_C - R_W)\exp(2R_C)\right) + R_W\frac{1-\exp(2(R_C - R_W))}{sh(2R_W)} \qquad (21)$$

Finally

$$R_C = d\frac{V_C}{2D} \text{ and } R_W = d\sqrt{\left(\frac{V_C}{2D}\right)^2 + \frac{i\omega}{D}} \qquad (22, 23)$$

In the above expressions D=diffusion coefficient; d,h,s= geometrical parameters of the transducer. Theoretical calculations of values of the transfer function $W(\omega, V_C) = I_W(\omega, V_C)/V_0(\omega)$ of the transducer at different levels of the constant electrolyte flow are plotted in Figure 9.

[1] Originally the general solution of this equation was obtained by the former PMD employee, Dr. Alex Panferov.

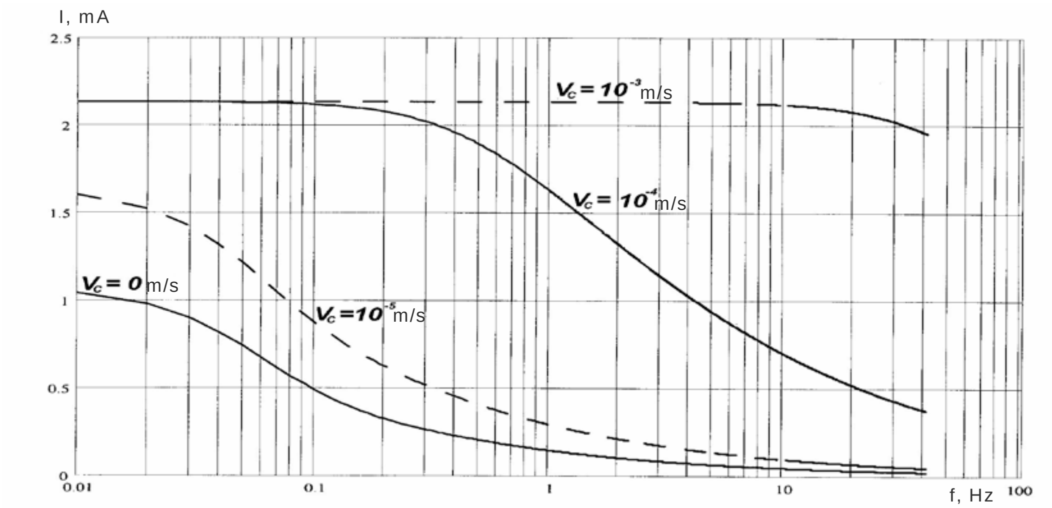

Figure 9. Transducer transfer function at different values of the permanent flow.

The plots clearly demonstrate that in the presence of a stationary flow of electrolyte the transfer coefficient of the electrochemical transducer increases while its passband extends farther toward the higher frequencies.

3. *Experimental Data*

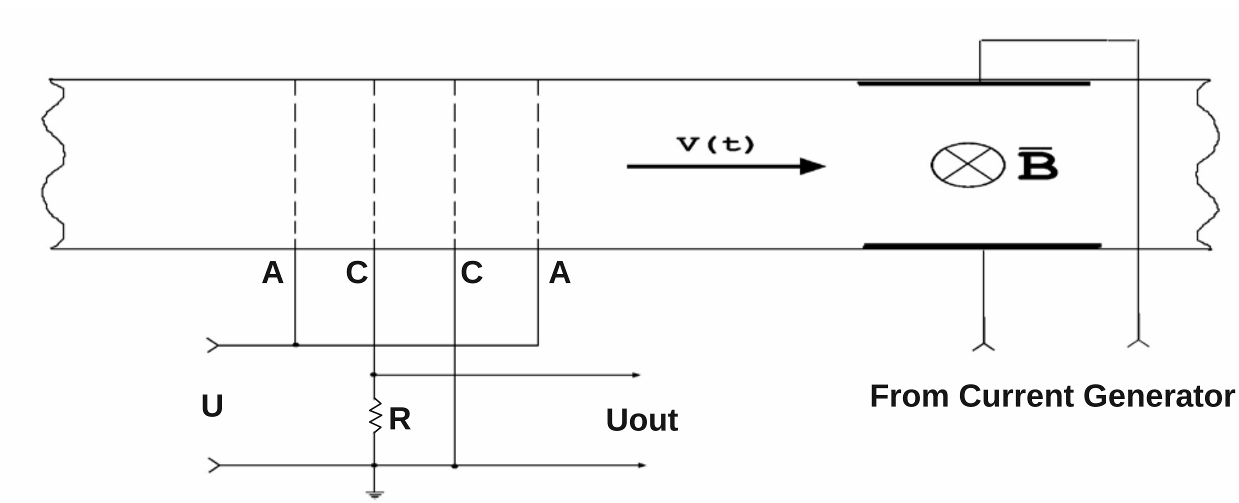

Figure 10: Experimental setup

A rotational sensor that is used in the current RSB20m rotational seismometer model was used in the experiments. The sensor consists of a polycarbonate toroidal channel filled with electrolyte. Built in the channel are a standard 4-electrode electrochemical transducer and an MHD cell. A constant voltage differential *U* was maintained between the cathodes and anodes. Transducer's output current generates voltage drop on the resistor R. This voltage war recorded into computer via a 22-bit ADC.

Both constant and modulating currents are injected into MHD electrodes. As a result, a force that is proportional to the cross product of the current density and magnetic induction is applied to the electrolyte. The pressure differential in the system generated by the moving liquid:

$$\Delta P = \frac{(\mathrm{B} \times \mathrm{I})L}{S} \qquad (24)$$

Where *L*=distance between electrodes and *S*=channel cross-section. Input signal of the transducer is the volumetric velocity, *q*, of the electrolyte that is related with the pressure differential in accordance with the Darcy law:

$$q = -\frac{\Delta P}{R_h} \tag{25}$$

Where R_h=hydraulic impedance of the toroid.

In the first set of experiments we measured dependence between the transducer's output current and the velocity of the stationary flow of the electrolyte. The theoretical curve is plotted on Figure 11; the crosses show experimentally measured values.

In the second set we measured transfer coefficient of the transducer versus the stationary flow velocity. These results are presented on Figure 12. The ordinates here are the ratios of the transducer transfer functions in the presence and absence of the electrolyte flow: $W(V_C)/W(0)$. The test data prove rather convincingly that when the stationary flow velocity is higher than 10^{-5} m/s the upper cutoff frequency becomes noticeably higher and that the overall transfer coefficient grows several times over. It is important to emphasize that these experimental results agree very well with the above presented theory in a very broad frequency range: from 0.01 to several tens of Hz.

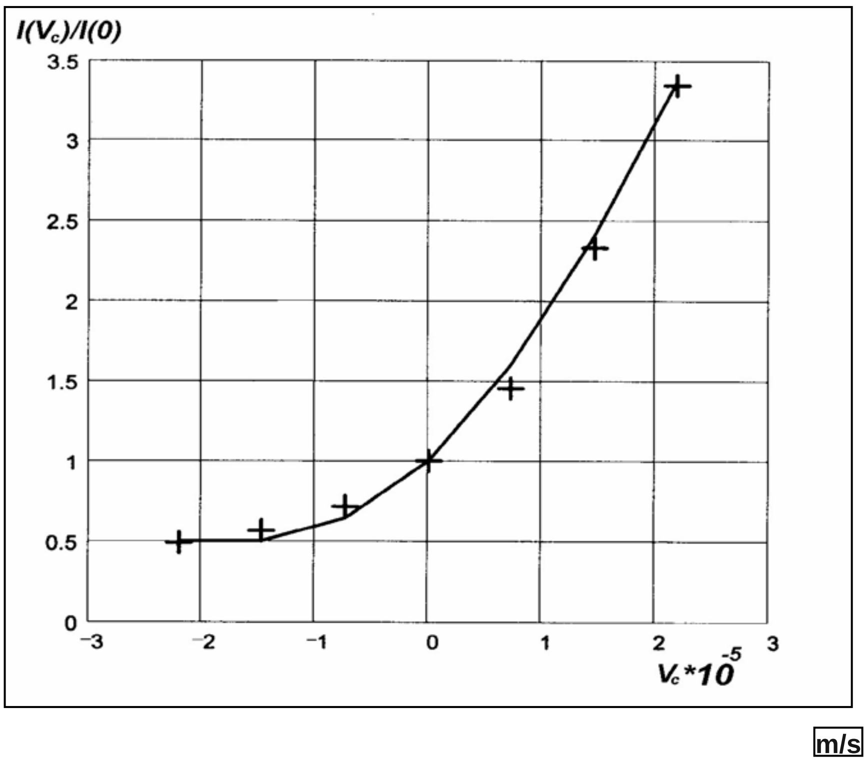

Figure 11. Transducer output current vs. the stationary flow velocity.

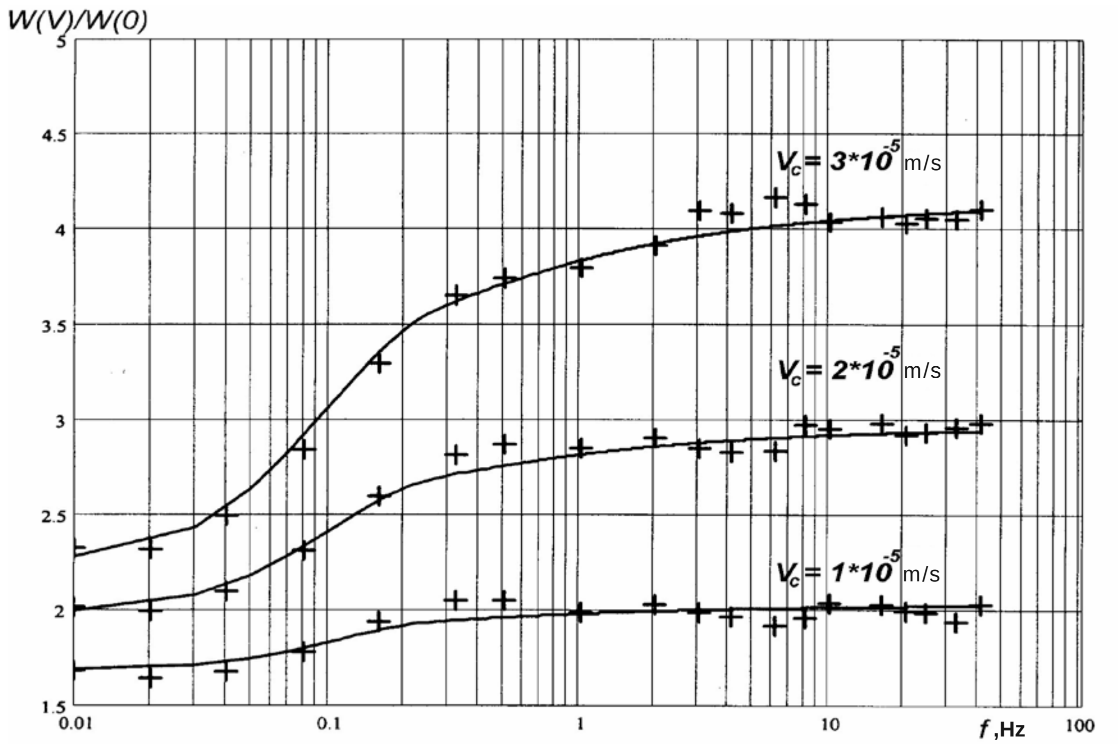

Figure 12. Transducer transfer coefficient vs. the stationary flow velocity.

F. Digitizer

This part of the project has been progressing rather smoothly and steadily. The block-diagram of the digitizer that is under development is shown below in Figure 13.

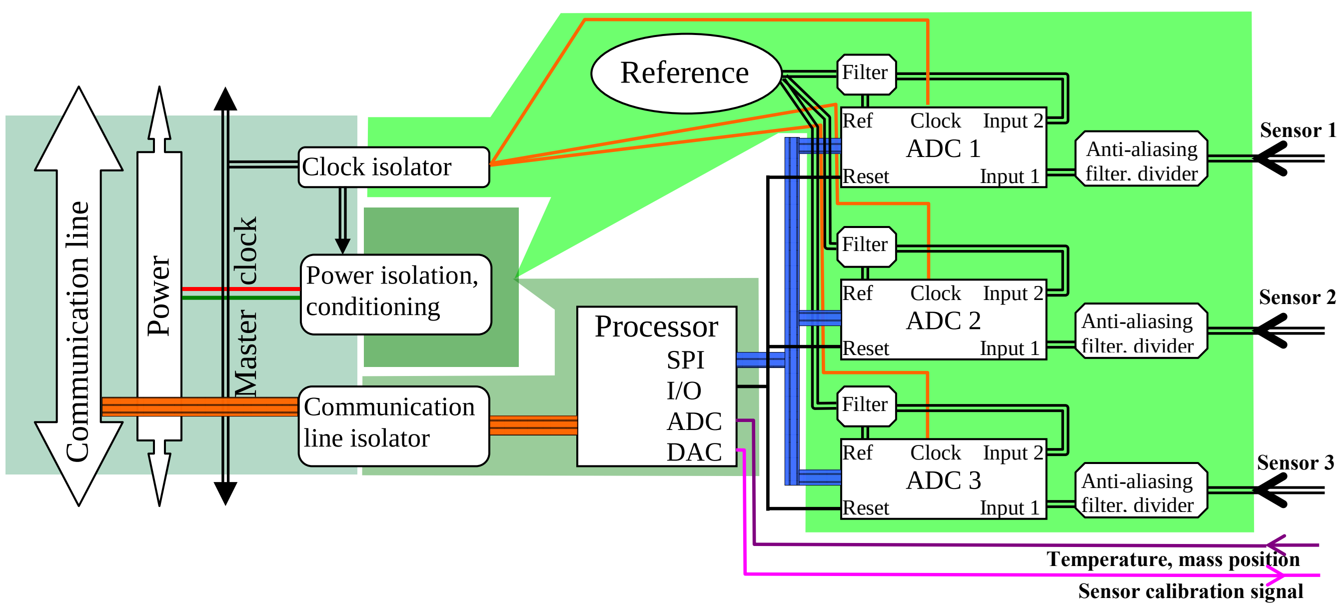

Figure 13. Digitizer Block Diagram

In order to make possible using the digitizer as a stand-alone device and/or work with other sensors the ‘Mass Position’ input (and ‘Mass Centering’ output not shown here) have been added. Also to allow for a multi-channel configuration the ‘Master Clock’ bus can be connected to similar digitizers in a common assembly.

An evaluation board for the Texas Instruments ADS1281/1282 has been purchased and used for the preliminary tests. A prototype board using TMS320VC5416 DSP and 3 ADS1282 converters was built and tested. The resulting noise was measured at ~1/3 bit higher than specified by TI.

An early decision had been made to have a dedicated microprocessor or a digital signal processor chip placed on the same board with the 3 channel converters. After an exhaustive search two possible processors have been selected for the final consideration: an MSP430 Ultra-low power microcontroller and a TMS320C55* low power DSP both manufactured by TI. While MSP430 offers several advantages, in particular, it had on-board ADC and DAC that can directly be used for state-of-health data recording, mass position readout, mass centering, etc. On the other hand, it seem unlikely that a microcontroller such as this one will be able to cope with extremely heavy computational load that is antialiasing filtering of three streams of data flowing with a maximum rate of up to 48 Kbaud. Therefore, at the moment we are inclined to use the above mentioned DSP even though additional 12-16 bit ADC/DAC chips will have to be deployed. Presently under development are the power regulators and clock circuits. Upon their completion the first three-channel prototype board will be built and tested.

CONCLUSIONS AND RECOMMENDATIONS

The first year of the Phase II project turned out to be more productive than anticipated. By the term “productive,” we do not necessarily mean only positive results. It is well known that some negative results going against the anticipated ones may turn out to be very useful. In our case such “failures” prompted us to perform a more thorough theoretical analysis and come up with more practical designs. Several sensor configurations were thoroughly analyzed; most of them have been built and tested. Most importantly, the experimental results in general showed close agreement with the theoretically predicted data albeit in a rather narrow passband. At the moment our first priority will be an exhaustive testing of the HEX prototype with a mini-membrane sensor. In the next step two prototypes will be built: one with the current distribution of the hydraulic impedance and another – with the low R_h sensor. If we are sufficiently satisfied with the laboratory test results to the point where we consider it worthwhile taking the prototype for the field tests at ASL it will be done. If we still feel that the further noise reduction is necessary we will start building and testing step be step other weapons from our arsenal, i.e., those described above combination sensor or/and the gyro device.

ACKNOWLEDGEMENTS

The authors are deeply grateful to Dr. Bob Hutt for his exceptional hospitality and highly qualified help during our trip to the ASL. Personal contacts with Drs. Mark Woods, Rick Schult, Preston Herrington, Yuri Starovoit and Prof. Erhard Wielandt greatly helped in formulating the requirements to and specifications of the new sensor.
Dr. Alexander Shilov of PMD Scientific played a leading role in data processing and analysis and in the development of the new digitizer.

REFERENCES

Abramovich I. and S. Daragan (1992). New family of inexpensive broad band seismometers, NSF SBIR Grant No. III-9360412, 1992-94

Koryta L. and K. Dvorak K. (1993). *Principles of Electrochemistry*, J. Wiley, New York.

Newman J. (1973). *Electrochemical Systems*, Prentice-Hall, Englewood Cliffs, New Jersey.

Sakharov K., (1992). Analysis of self-noise of molecular electronic seismic sensors, in *Proceedings MIPT*, vol.26, No.3, 1992 (in Russian)

Van der Ziel A. (1970). Noise; sources, characterization, measurement, Prentice Hall, 1970